Rev. Roum. Sci. Techn.– Électrotechn. et Énerg.
Vol. **64**, *2*, pp. 113–118, Bucarest, 2019

ACCUMULATION AND EFFECTS OF SPACE CHARGE IN DIRECT CURRENT CABLE JOINTS. PART I: MODEL AND METHODS FOR SPACE CHARGE DENSITY COMPUTATION

LUCIAN VIOREL TARANU, PETRU V. NOTINGHER, CRISTINA STANCU

Key words: Dc cable joints, Cross-linked polyethylene, Ethylene-propylene rubber, Space charge, Electric field, Electrical conductivity.

Part I of this paper presents a cylindrical two-layer insulation model and two methods (A and B) for determining the space charge density in the insulation (dual insulation) of dc cable joints. The method A is based on the material parameters (electrical conductivity and permittivity) and the method B - on electroacoustic pulses. The values of the electrical conductivity for different temperatures and electric fields are computed using some experimental results and equations specific to each material. The equations used to compute the electrical conductivity, the electrical field and the superficial space charge densities at the interfaces between the joint's insulation layers are also presented. Finally, the values and the variations of the electrical conductivity with the electric field and temperature are presented and analyzed.

1. INTRODUCTION

Due to the remarkable advantages that dc power transmission has, compared to that in ac, (higher energy transmission capacity, lower conductor losses, no electromagnetic interference and skin effect, low corona effect losses, reduced magnetic field, lower impact on the environment, etc.), over the last few years there have been considerable developments (in Europe, Asia and North America) of networks of polymeric insulated cables that can operate at very high voltages (from 500 kV currently and up to 800 or even 1100 kV) in the near future [1, 2]. Since the sections of high voltage cables have reduced lengths (1 ... 10 km), for the transmission of energy over long distances several sections are required, connected together with joints [2]. In the last decade, great efforts have been made to develop joints with extruded polymeric insulation materials, such as XLPE, EPDM, EPR, silicone rubber etc. (Fig. 1, [3]).

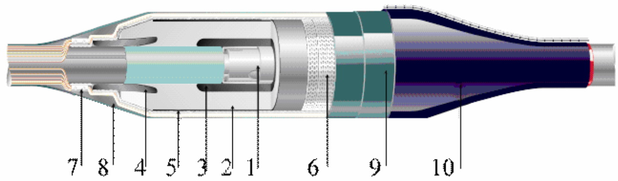

Fig. 1 – Cross section through a one-piece joint (for 245 kV): 1- Shear bolt connector; 2- Insulating joint body; 3- Inner electrode; 4- Deflector; 5- Exterior semiconductor screen; 6- Copper shielding sock; 7- Screen connection; 8- Mastic; 9- Insulating sleeves; 10- Outer protection [3].

On the other hand, consumer demand for the quality of energy provided by the energy suppliers has considerably increased. The availability of an energy supply system is one of the key factors in establishing a power supply, and the availability values required today are very high: a domestic user in the EU requires a 99.98 % availability, whilst an industrial one requires 99.996 % [4]. An ideal power supply is that which is always available, with the voltage and frequency within acceptable limits and with a pure sinusoidal voltage wave [1].

The most obvious electric power failures are power outages (power interruptions from a few seconds to several hours) and voltage dips (where the voltage reaches a low value for short duration (from 10 ms to 60 s)) [4]. Obviously, long-term interruptions are a problem for all consumers, but many operations are very sensitive even at very short interruptions: continuous flow processes (paper industry etc.), successive and continuous operations, or in many stages (semiconductor industry etc.), data processing (stock exchanges, value exchanges etc.) etc. The statistics made in last year's shows that joints are responsible for 52 % of premature removal from operation of transmission and distribution lines of electricity (Fig. 2, [5]).

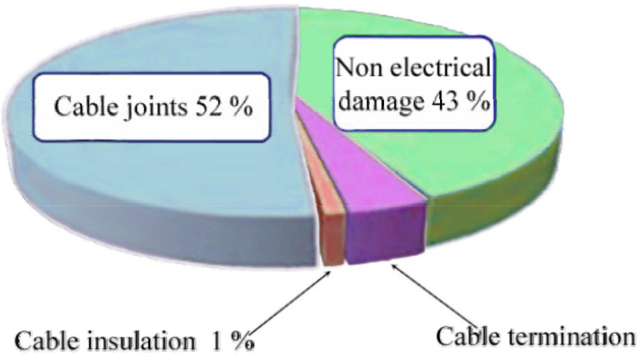

Fig. 2 – Statistical distribution of cable failure causes [5].

Premature failure of the joint is due, especially, to the degradation of the insulation [6], generated by the intensification of the thermal, electrical and mechanical stresses during operation. This intensification is due to manufacturing defects (peeling of insulation layers, cavities, impurities etc.), partial discharges, charge injection from electrodes, separation of space charge in the bulk and at the interfaces of insulation layers, local increases of temperature etc. The accumulation of space charge in the volume of the insulation is due to the byproducts resulted from the technological processes of their manufacture, charge injection from electrodes, chemical degradation (fracture of the molecules) of the insulation, development of electric and water trees etc., and has as a main effect the local intensification of the electric field during the operation of the joint and, of course, of the residual electric field (after the power-off of the cable lines of which the joints are a part of). Or, the increases of the residual electric field values could be extremely hazardous for dc joints operating at high and extremely high voltages.

"POLITEHNICA" University of Bucharest, MMAE Dept., Romania. E-mail: lvtaranu@elmat.pub.ro

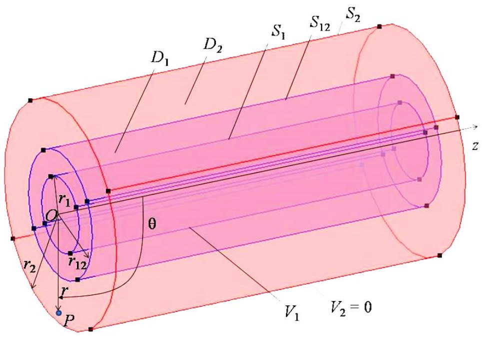

Fig. 3 – Computation domain of the electric field.

On the other hand, as polymeric materials used for the joints have different physical and electrical properties (electrical conductivity and permittivity), during cable operation, at the insulator-insulator interfaces superficial space charge of density ρ_s is separated [7, 8]. Using an analytical expression of ρ_s, several researchers have tried to determine its values at the interfaces between layers of cross-linked polyethylene (XLPE) and ethylene-propylene-diene-monomer rubber (EPDM) or ethylene-propylene rubber (EPR) [9, 10].

During operation, new charge carriers appear, the space charge density increases, both inside the homogeneous areas and at the interfaces between them. Unlike the operation in ac, in dc the space charge accumulates continuously, producing a supplementary electric field that exceeds the field corresponding to the voltage at which the cable operates [11]. The accumulation of space charge is, also, closely linked to the quality of the interface between the two insulating materials (surface roughness [12] etc.), influenced by the technological parameters (pressure, temperature) of joint manufacture [13]. Therefore, in some areas of joint insulation (near the interfaces between heterogeneous areas, in cavities etc.) the electric field greatly intensifies, reaching values several times higher than those existing in the absence of charge. As a result, there is an increase in partial discharges and a reduction in the inception voltage of the electrical and water trees, and, respectively, insulation breakdown.

The electric field was computed considering different models. Thus, using a finite element analysis software, Illias [14] and He [15] took into consideration defects in insulation, Notingher [16–18] – the existence of electrode protuberances and gas cavities in the insulation, Lachini [19] – the existence of moisture in cavities, Bodega [7] and Fothergill [20] – the existence of space charge, Notingher [21] and Stancu [22, 23] – the existence of space charge corresponding to the development of water trees in cables etc.

In previous works [2, 24–26], the influence of the properties of the insulation components of a joint on the accumulation of space charge at the interface was analyzed, and the electric field distribution was calculated.

In this paper, for the computation of the superficial charge density accumulated at the interface of a joint cable model layers two methods are presented. The first one (A) uses an equation that includes the material parameters (the electrical permittivity and conductivity) and the second one (B) is based on the use of some electroacoustic pulses. In Part I, only the methods and equations used for space charge density determination are described. Also here, the variations of the electrical conductivity for different temperatures and electric fields are shown and analyzed.

The results regarding the superficial charge density are presented and discussed in Part II.

2. COMPUTATION OF THE CHARGE DENSITY

2.1. METHOD A

2.1.1. ELECTRIC FIELD AND CHARGE DENSITY

Because the electrical conductivity depends on the electric field, the computation of the field is needed. The computation of the electric field E and surface charge density ρ_s were performed in a cylindrical domain $D = D_1 \cup D_2$, consisting of subdomains D_1 (of thickness g_1,relative permittivity ε_{r1} and dc conductivity σ_{dc1}) – delimited by the surfaces S_1 (of radius r_1) and S_{12} (of radius $r_{12} = r_1 + g_1$) – and D_2 (of thickness g_2, relative permittivity ε_{r2} and conductivity σ_{dc2}) – delimited by the surfaces S_{12} and S_2 (of radius $r_2 = r_1 + g_1 + g_2$) (Fig. 3). All the cylindrical surfaces $S_{1,12,2}$ have the same generator of length l, higher than their radii. A value of potential V_1 has been assigned to S_1, whilst a value $V_2 = 0$ (ground potential) has been set on S_2.

2.1.2. EQUATIONS

Considering the domain D linear, isotropic and inhomogeneous, respectively

$$\overline{D}(P) = \varepsilon(P)\overline{E}(P), \quad P \in D\,, \tag{1}$$

$$\overline{J}(P) = \sigma(P)\overline{E}(P), \quad P \in D\,, \tag{2}$$

and the electrostatic generalized field regime, the following equations were used:

- *Electric flux law*:

$$\mathrm{div}\overline{D}(P) = \rho_v(P), \quad P \in D\,, \tag{3}$$

- *Charge conservation law*:

$$\mathrm{div}\overline{J}(P) + \frac{\partial \rho_v(P)}{\partial t} = 0, \quad P \in D\,, \tag{4}$$

- *Potential theorem:*

$$\overline{E}(P) = -\mathrm{grad}V(P), \quad P \in D \tag{5}$$

where $\overline{D}(P)$ represents the electric induction, $\overline{E}(P)$ – electric field, $\overline{J}(P)$ – electric current density, $\rho_v(P)$ – volume charge density, $V(P)$ – electric potential, $\varepsilon(P)$ – electrical permittivity and $\sigma(P)$ – electrical conductivity in a point $P \in D$ at time t.

2.1.3. BOUNDARY CONDITIONS

On the surfaces S_1 and S_2 Dirichlet conditions were imposed at each time t:

$$V(M) = V_1, \quad M \in S_1\,, \tag{6}$$

$$V(M) = V_2, \quad M \in S_2\,. \tag{7}$$

On the discontinuity surface S_{12} the following conditions were imposed at each time t:

$$\bar{n}_{12}\left(\bar{J}_2(M)-\bar{J}_1(M)\right)+\frac{\partial \rho_s(M)}{\partial t}=0,\quad M\in S_{12}, \tag{8}$$

$$\left(\varepsilon_1\frac{\partial V_1(M)}{\partial n_{12}}-\varepsilon_2\frac{\partial V_2(M)}{\partial n_{12}}\right)=\rho_s(M),\ M\in S_{12}, \tag{9}$$

where $\bar{n}_{12}$ is the normal versor on S_{12}, $\rho_s(M)$ represents the surface charge density in a point $M \in S_{12}$ at time t, $\varepsilon_{1,2} = \varepsilon_{r1,2}\cdot\varepsilon_0$ and ε_0 is the vacuum permittivity.

2.1.4. INITIAL CONDITIONS

It is considered that, at the moment of applying the voltage ($t = 0$), there is no electric charge on the discontinuity surface S_{12}, respectively that:

$$\rho_s(M)\big|_{t=0}=0,\ M\in S_{12}. \tag{10}$$

2.1.5. MATERIAL PROPERTIES

To initialize the computation of the electric field, the values of dc conductivity (σ_{dc}) and relative permittivity (ε_r) are needed. The electrical conductivity was determined by experiments at various voltages between 1 kV and 20 kV (denoted by σ_A for EPR and σ_B for XLPE, the values presented in [10, 27]) and the real part of complex relative permittivity (denoted by ε_A for EPR and ε_B for XLPE) was measured at 50 Hz, with values presented in Table 1.

The values of ε_r were considered independent on the thermodynamic temperature T and on the electric field E. For the conductivity it was considered that the influence of T and E cannot be neglected, respectively that σ has an expression of the following form [30]:

$$\sigma(E,T)=Af_T(T)f_E(E), \tag{11}$$

where $A=\prod_i f_{C_i}(C_i)$, and f_{C_i}, f_E and f_T are dependent functions on the charge carriers concentrations C_i, on E and, respectively, on T.

In this paper it was considered that the values of C_i are constant in regards to E and T and σ was computed in D_1 with equation

$$\sigma_A(E,T)=A_A\exp\left(-\frac{E_{a,A}}{kT}\right)\frac{\sinh\left((a_AT+b_A)\ln E\right)}{E^{\alpha_A}}, \tag{12}$$

proposed by the authors, for EPR, in [10], and in D_2 with the equation

$$\sigma_B(E,T)=A_B\exp\left(-\frac{E_{a,B}}{kT}\right)\frac{\sinh\left((a_BT+b_B)\ln E\right)}{E}, \tag{13}$$

proposed by the authors, for XLPE, in [27], where $\sigma_{A,B}(E,T)$ represents the conductivity in a point, $E_{aA,B}$ – activation energies, $A_{A,B}$, $a_{A,B}$, $b_{A,B}$ and α_A – material constants for EPR (A) and XLPE (B) (Table 1), T – temperature (measured in K), $T = \theta + 273.15$ and $k = 1.38.10^{-23}$ J/K – the Boltzmann's constant.

Table 1

Values of ε_r, E_a, A, a, b and α for samples A and B

Sample	ε_r (-)	E_a (eV)	θ (°C)	A (S/m)	a (m/K^{-1})	b (-)	α (-)
A (EPR)	2.77	0.6	≤ 50	0.24 μ	1.6	0.16	0.21
			≥ 50	5.47 n	6.5	–1.17	0.23
B (XLPE)	2.19	0.55	≤ 50	0.95 f	–3.4	3.406	1
			≥ 50	0.95 f	–2.37	3.069	1

2.1.6. CHARGE DENSITY

The value of the surface charge density $\rho_s(t)$, separated at the instant t after applying the voltage $U = V_1 - V_2$ at the S_{12} interface, has been calculated with the equation [8]:

$$\rho_{s,cal}(t)=\varepsilon_B E_2(r_{12},t)-\varepsilon_A E_1(r_{12},t), \tag{14}$$

where $E_{1,2}(r_{12},t)$ represents the values of E on the S_{12} interface at instant t.

2.1.7. ELECTRIC FIELD

Considering that the material parameters (ε and σ) are constant in $D_{1,2}$ and that, at instant $t = 0$, at the S_{12} interface there is no electric charge (respectively, $\rho_s(0) = 0$), using equations (1), (3) and (5), the electric field expressions (15) – in D_1 – and (16) – in D_2 – have been obtained.

$$E_1(t)=\frac{U}{r}\left[\left(\frac{\varepsilon_B}{\varepsilon_A\ln\frac{r_2}{r_{12}}+\varepsilon_B\ln\frac{r_{12}}{r_1}}-\frac{\sigma_B}{\sigma_A\ln\frac{r_2}{r_{12}}+\sigma_B\ln\frac{r_{12}}{r_1}}\right)e^{-t/\tau}+\frac{\sigma_B}{\sigma_A\ln\frac{r_2}{r_{12}}+\sigma_B\ln\frac{r_{12}}{r_1}}\right], \tag{15}$$

$$E_2(t)=\frac{U}{r\ln\frac{r_2}{r_{12}}}-\frac{U}{r}\frac{\ln\frac{r_{12}}{r_1}}{\ln\frac{r_2}{r_{12}}}\left[\left(\frac{\varepsilon_B}{\varepsilon_A\ln\frac{r_2}{r_{12}}+\varepsilon_B\ln\frac{r_{12}}{r_1}}-\frac{\sigma_B}{\sigma_A\ln\frac{r_2}{r_{12}}+\sigma_B\ln\frac{r_{12}}{r_1}}\right)e^{-t/\tau}+\frac{\sigma_B}{\sigma_A\ln\frac{r_2}{r_{12}}+\sigma_B\ln\frac{r_{12}}{r_1}}\right] \tag{16}$$

With the equations (15) and (16) the values of the electric field $E(t)$ can be calculated in any point from D, and with (14) – the charge density at the interface S_{12} ($\rho_s(t)$).

As σ depends on E (respectively, on r), analytical expressions of the electrical field cannot be obtained, and the computation of its values was performed using a numerical method, utilizing the COMSOL Multiphysics® software. The equations (15) and (16) were used to initiate the numerical calculation program of the electric field.

2.2. METHOD B

Method B uses some electroacoustic pulses that allow measuring a volume space charge density (ρ_v). The volume density of space charge in our models was measured using a pulsed electroacustic (PEA) space charge measuring setup at the Laboratory of Innovation Technology (LIT), University of Bologna [29], in the absence and in the presence of various dc voltages (under 100 kV), on cylindrical samples described in subparagraph 3.1 of the paper. The PEA signal has been acquired at different time instants (faster in the beginning – approx. 1 second apart – and slower – approx. 1 minute apart – at about 1 hour of measurement time) on an oscilloscope controlled with an application using the LABVIEW software. The PEA measurement results (the volume density of space charge, ρ_v) were elaborated from the acquired signal using a deconvolution and calibration procedure for cylindrical samples using a GUI application in the MATLAB software.

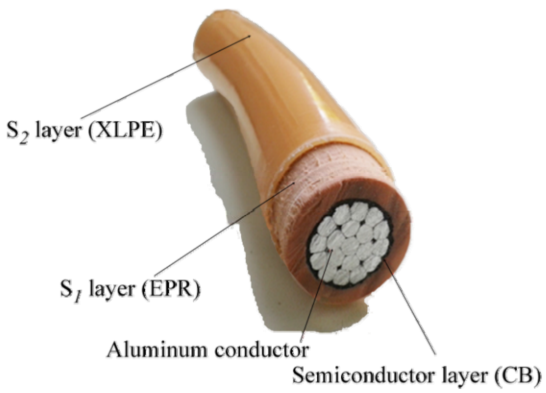

Fig. 4 – Cylindrical EPR/XLPE sample.

Knowing the experimental values of ρ_v, the values of ρ_s (respectively, $\rho_{s,exp}$) were determined with the equation:

$$\rho_{s,exp} = \left(2\int_{r_a}^{r_b} \rho_v(r) r \mathrm{d}r \right) / (r_a + r_b) \qquad (17)$$

where r_a and r_b represent the radii of cylindrical surfaces very close to each other, located at an equal distance on both sides of the S_{12} interface.

3. **EXPERIMENTS**

The dc electrical conductivity σ_{dc} and relative permittivity ε_r were determined experimentally on flat samples of EPR (of average thickness $g_1 = 0.484$ mm) and XLPE (of average thickness $g_2 = 0.304$ mm). The computation of σ values for different values of the temperature and electric field was done on the cylindrical joint model presented in subparagraph 2.1.1, with a geometry close to that of the cylindrical samples.

The cylindrical samples have the conductor from aluminum strands (with a diameter of 14 mm), a layer of semiconductor from carbon black (CB) polyethylene (of thickness 0.7÷1 mm), a layer of ethylene-propylene rubber S_1 (EPR) (of thickness 3.3÷3.7 mm) and a layer of cross-linked polyethylene S_2 (XLPE) (of thickness 1÷1.2 mm) (Fig. 4). All samples were manufactured at ICME ECAB SA Bucharest, and the manufacturing method is presented in [28].

The manufacturing and conditioning procedures used for the flat samples are presented in [10] for EPR and in [27] for XLPE. The measurement of the ε_r values was performed using a Novocontrol impedance analyzer at the Politehnica University of Bucharest (UPB) and for the electrical conductivity a Keithley electrometer connected to a setup at LIT was used (at variable temperatures and electric fields [10]).

Based on the conductivity variation curves obtained at 3 temperatures (30, 50 and 70 °C) and 4 values of the electric field (5, 10, 15 and 20 MV/m) ([10, 27]) and equations (12) and (13), using the Matlab software (with the *fsolve* function from the *Optimization Toolbox* package) the $E_{aA,B}$, $A_{A,B}$, $a_{A,B}$, $b_{A,B}$ and α_A constants were calculated (Table 1).

4. **RESULTS**

Introducing these values in equations (12) and (13), the values of the electrical conductivity for different temperatures up to 90 °C and electric field values were computed. A part of the results are presented in Figs. 5–8.

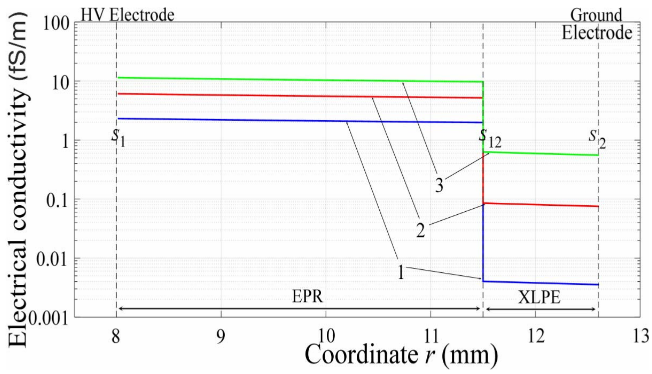

Fig. 5 – Variation of the electrical conductivity with coordinate r for $t = 1$ s (**1**), 10 s (**2**) and 60 s (**3**) (Voltage On, $U = 50$ kV, $\theta = 30$ °C).

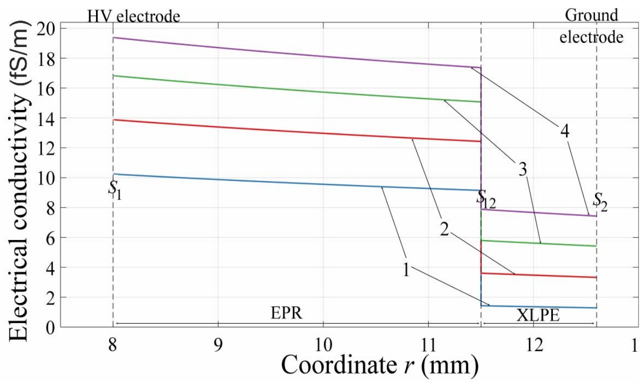

Fig. 6 – Variation of the electrical conductivity with coordinate r for $U = 25$ (**1**), 50 (**2**), 75 (**3**) and 100 (**4**) kV (Voltage On, $t = 3600$ s, $\theta = 30$ °C).

Figures 5 and 6 show the variation of the electrical conductivity σ with the radial coordinate r at $T = 30$ °C and $U = 50$ kV for different moments (Fig. 5) and at different applied voltages for $t = 3600$ s (Fig. 6), in the absence of volume charge ($\rho_v(r,t) = 0$), but in the presence of superficial charge on S_{12} ($\rho_s(t) \neq 0$). It is found that the conductivity decreases slowly with the increase of r, due, probably, to the decrease with r for the electric field E. Also, the conductivity is found to increase in both layers as the applied voltage increases from 25 to 100 kV, having values roughly two times higher in EPR and four times higher in XLPE at $U = 100$ kV from $U = 25$ kV (Fig. 6).

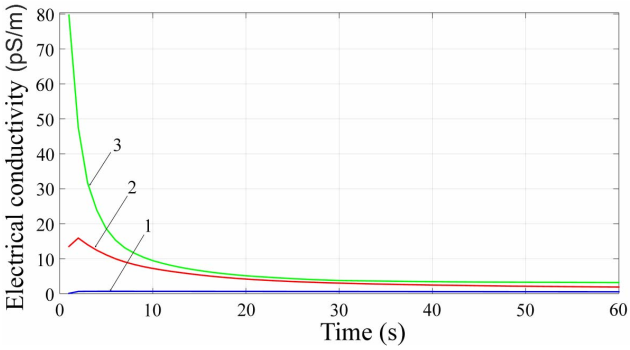

Fig. 7 — Variation of the electrical conductivity with time in EPR at the interface S_{12}, for θ = 60 °C (1), 80 °C (2) and 90 °C (3) (Voltage On, $U = 50$ kV).

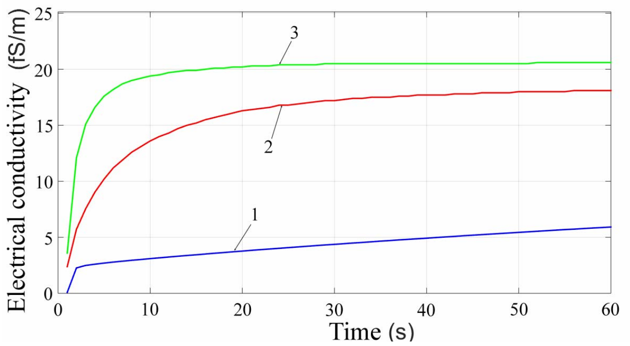

Fig. 8 — Variation of the electrical conductivity with time in XLPE at the interface S_{12}, for θ = 60 °C (1), 80 °C (2) and 90 °C (3) (Voltage On, $U = 50$ kV).

Immediately after applying the voltage, at the points in EPR adjacent to the S_{12} interface there is an important increase in the electrical conductivity (Fig. 7), followed by a reduction of its values to the steady state. In the case of XLPE, in the first seconds there is a pronounced increase in conductivity (Fig. 8), followed by a slow increase when its values stabilize. This is due, most likely, to the increases with time of the electric field values.

When the temperature increases from 60 to 90 °C, the electrical conductivity at the points adjacent to the S_{12} interface increases (Figs. 7 and 8). For example, for $t = 60$ s, σ increases 6 times in EPR and 3.5 times in XLPE (Figs. 7 and 8). These increases of σ, highlighted in equations (12) – (13), are due to the temperature rise of the values of the own energies of charge carriers [7].

For the calculation of the electric field $E(t)$ and the superficial charge density ($\rho_{s,cal}$) at the interfaces of samples at instant t, the values of the conductivity determined at that instant ($\sigma(t)$) were used. The values of E and $\rho_{s,cal}$ will be presented in the Part II of the paper.

5. CONCLUSIONS

The cylindrical two-layer insulation models of joints allow to calculate the space charge density at the interfaces of dc cable joints.

As space charge density depends on the electric field and material properties (electric conductivity and permittivity) values, the electric field and the electric conductivity were calculated and their variations with temperature was shown.

Increasing the temperature and the electric field leads to a considerable increase (with approx. 3 – 4 orders of magnitude) in the electrical conductivity of the insulating layers. As the variations with temperature for the permittivity are less important than those of the conductivity, the increase of the conductivity leads to a significant increase of the superficial charge density, and, thus, of the electric field in the cable joints (see Part II).

Received on April 7, 2019

REFERENCES

1. C. Kim, V. Sood, G. Jang, S. Lim, S. Lee, *HVDC transmission: power conversion applications in power systems*,Wiley Press, 2009.
2. C. Stancu, P. V. Notingher, L. V. Taranu, A. Cernat, A. Constantin, *Influence of the properties of the joint insulation components on the space charge and electric field*, J. Int. Sci. Publ. : Mater. Methods Technol., **11**, pp. 76–91, 2017.
3. *** TE Connectivity, *High Voltage Cable Accessories up to 245 kV*.
4. D. Chapman, *The cost of a not satisfactory energy quality*, SIER Press, Bucharest, 2001.
5. E. Gulski, W. Boone, E.R.S. Groot, J. Pellis, B.J. Grotenhuis, F.J. Wester, N. Schaik, E.F. Steenis, *Knowledge rules support for CBM of power cable circuits*, CIGRE, Paris, SC 15, Paper 104, 2002.
6. J. Fothergill, *Ageing, Space Charge and Nanodielectrics: Ten Things We Don't Know About Dielectrics*, International Conference on Solid Dielectrics, pp. 1–10, 2007.
7. R. Bodega, *Space charge accumulation in polymeric high voltage DC cable systems*, Ph.D Thesis, Delft University, Netherlands, 2006.
8. P.V. Notingher, *Materials for electrotechnics*, POLITEHNICA Press, Bucharest, 2005.
9. L. Boyer, J. Matallana, J. F. Brame, J. Castellon, P. jr. Notingher, S. Agnel, A. Toureille, *Electric field measurements on XLPE/EPDM layer insulation system under DC stress*, Proc. JICABLE, Paper B.4.2., 2011.
10. L.V. Taranu, P.V. Notingher, C. Stancu, *Dependence of Electrical Conductivity of Ethylene-Propylene Rubber on Electric Field and Temperature*, Rev. Roum. Sci. Techn. – Électrotechn. Et Énerg, **63**, *3*, pp. 243–248, 2018, ISSN 0035-4066.
11. C. Stancu, P. V. Notingher, P. jr. Notingher, *Computation of the Electric Field in Aged Underground Medium Voltage Cable Insulation*, IEEE Trans. Dielectr. Electr. Insul., **20**, *5*, pp. 1530–1539, 2013.
12. V. Homburg, H. C. Karner, *Basic investigation of a macroscopic interface between two solid dielectrics*, Conf. Record of the 1994 IEEE Int. Symp. on El. Insul., pp. 446–449, 1994.
13. *** S. Ansorge, B. Arnold, *Jointing of high voltage cable systems*.
14. H. A. Ilias, Q. L. Ng, A. H. A. Bakar, H. Mokhlis, A. M. Ariffin, *Electric field distribution in 132 kV XLPE cable termination model from finite element method*, Proc. of the Int. Conf. on Cond. Monitor. and Diag. (CMD), 2012, pp. 80–83.
15. M. He, G. Chen, P. Lewin, *Field distortion by a single cavity in HVDC XLPE cable under steady state*, IET Journals, **1**, *3*, pp. 107–114, 2016.
16. P.V. Notingher, D. Ioan, *A Numerical Method for Computing the Electrical Stress in Dielectrics*, Rev. Roum. Sci. Techn. – Électrotechn. Et Énerg., **23**, *3*, pp. 363–372, 1978.
17. P.V. Notingher, *Méthodes de calcul de la dureé de rupture dans le systeme pointe-plan*, Rev. Roum. Sci. Techn. – Électrotechn. Et Énerg., **31**, 1, pp. 59–68, 1986, ISSN 0035-4066.
18. P.V. Notingher, *Le calcul des dureés de rupture des dielectriques solides. L'infuence des gas de l'interieur des caviteés*, Rev. Roum. Sci. Techn. – Électrotechn. Et Énerg., **31**, *2*, pp. 133–144, 1986.
19. S. Lachini, A. Gholami, *The simulation of electric field distribution on cable under the presence of moisture and air voids*, Proc. of the 4th Int. Power Eng. Optim. Conf. (PEOCO), pp. 149–153, 2010.
20. J. Fothergill, *The Coming of Age of HVDC Extruded Power Cables*, Electrical Insulation Conference, pp. 124–137, 2014.
21. P.V. Notingher, I. Radu, J.C. Filippini, *Numerical Method of Computation of the Electric Field in Insulation with Water-Trees. Part I: Computation Methods*, Rev. Roum. Sci. Techn. – Électrotechn. Et Énerg., **45**, *2*, pp. 221–236, 2000.
22. C. Stancu, P.V. Notingher, F. Ciuprina, P. Notingher jr, S. Agnel, J. Castellon, A. Toureille, *Computation of the Electric Field in Cable*

Insulation in the Presence of Water Trees and Space Charge, IEEE Trans. Ind. Appl., **45**, *1*, pp. 30–49, 2009.
23. C. Stancu, P.V. Notingher, P. Notingher jr., *Influence of Space Charge Related to Water Trees on the Breakdown Voltage of Power Cable Insulation*, J. of Electrost., **71**, *2*, pp.145–154, 2013.
24. C. Stancu, P. V. Notingher, L. V. Taranu, *Concerning the space charge accumulation in DC power cable joints insulation*, J. Int. Sci. Publ. : Mater. Methods Technol., **10**, pp. 154–174, 2016.
25. C. Stancu, P. V. Notingher, P. jr. Notingher, M. Lungulescu, *Space charge and electric field in thermally aged multilayer joints model*, IEEE Trans. Dielectr. Electr. Insul., **23**, *2*, pp. 633–644, 2016.
26. L.V. Taranu, P. V. Notingher, C. Stancu, *Concerning the separation of space charge at the DC cable joints interfaces*, Proc. of Inter. Symp. on Fundam. of El. Eng. (ISFEE), Bucharest, Paper 533-1889-1-SP, 2018.
27. L.V. Taranu, P.V. Notingher, C. Stancu, *The Influence Of Electric Field And Temperature On The Electrical Conductivity Of Polyethylene For Power Cable Insulations*, U.P.B. Sci. Bull, **80**, *4*, pp. 45–56, 2018, ISSN 1223-7027.
28. C. Stancu, *Report no 2 – Reduction of space charge in composite insulations of HVDC cable joints*, Research project PN-II-RU-TE-2014-4-0280, 2016.
29. R. Bodega, P.H.F. Morshuis, J.J. Smit, *Space charge measurements on multi-dielectrics by means of the pulsed electroacoustic method*, IEEE Trans. Dielectr. Electr. Insul., **13**, *2*, pp. 272–281, 2006.
30. H. Ghorbani, M. Jeroense, C. Olsson, M. Saltzer, *HVDC Cable Systems - Highlighting Extruded Technology*, IEEE Trans. Power Del., **29**, *1*, pp. 414–421, 2014.